TISSUE ENGINEERING: Part A
Volume 19, Numbers 13 and 14, 2013

DOI: 10.1089/ten.tea.2012.0377

Glycosaminoglycan Mimetic Associated to Human Mesenchymal Stem Cell-Based Scaffolds Inhibit Ectopic Bone Formation, but Induce Angiogenesis *In Vivo*

Guilhem Frescaline, PhD,[1,2] Thibault Bouderlique, PhD,[1,2] Leyya Mansoor, MS,[1,2] Gilles Carpentier, MS,[1,2] Brigitte Baroukh, PhD,[3] Fernando Sineriz, PhD,[4] Marina Trouillas, PhD,[5] Jean-Louis Saffar, PhD,[3] José Courty, PhD,[1,2] Jean-Jacques Lataillade, PhD,[5] Dulce Papy-Garcia, PhD,[1,2] and Patricia Albanese, PhD[1,2]

Tissue engineering approaches to stimulate bone formation currently combine bioactive scaffolds with osteocompetent human mesenchymal stem cells (hMSC). Moreover, osteogenic and angiogenic factors are required to promote differentiation and survival of hMSC through improved vascularization through the damaged extracellular matrix (ECM). Glycosaminoglycans (GAGs) are ECM compounds acting as modulators of heparin-binding protein activities during bone development and regenerative processes. GAG mimetics have been proposed as ECM stabilizers and were previously described for their positive effects on bone formation and angiogenesis after local treatment. Here, we developed a strategy associating the GAG mimetic [OTR_{4120}] with bone substitutes to optimize stem cell-based therapeutic products. We showed that [OTR_{4120}] was able to potentiate proliferation, migration, and osteogenic differentiation of hMSC *in vitro*. Its link to tricalcium phosphate/hydroxyapatite scaffolds improved their colonization by hMSC. Surprisingly, when these combinations were tested in an ectopic model of bone formation in immunodeficient mice, the GAG mimetics inhibit bone formation induced by hMSC and promoted an osteoclastic activity. Moreover, the inflammatory response was modulated, and the peri-implant vascularization stimulated. All together, these findings further support the ability of GAG mimetics to organize the local ECM to coordinate the host response toward the implanted biomaterial, and to inhibit the abnormal bone formation process on a subcutaneous ectopic site.

Introduction

To induce bone formation, tissue engineering is currently investigating the feasibility to associate biomaterials to stem cell therapeutic products, such as human mesenchymal stem cells (hMSC) committed to an osteogenic phenotype.[1,2] One rational challenge in this area is to create scaffolds that could provide an appropriate extracellular matrix (ECM) for efficient adhesion, survey, proliferation, and differentiation of therapeutic cellular products that will be further applied to an injured tissue. However, perfect mimicry is difficult to achieve, considering the complex molecular, cellular, and mechanical processes requiring being timely coordinated for tissue repair. Synthetic bone substitutes such as tricalcium phosphate/hydroxyapatite (TCP/HA) ceramics have been developed because of their bioactive and osteoconductive properties,[3] and bone marrow MSC loaded on such porous ceramics have shown efficacy in some clinical trials.[4,5] However, these products still need to be improved, for example, *in vitro* process of scaffold colonization by hMSC, to overcome specific pitfalls for large-scale implementation of clinical applications. Also, angiogenesis is crucial for the formation of a functional microvasculature network supplying the devices in nutrients, allowing cellular survival into the damaged matrix.[6,7] Thus, tissue engineering strategies aim to recreate complex niches optimized to stabilize endogenous or therapeutic growth factors and to preserve or potentiate therapeutic cells properties.[8,9]

Among the major components of the ECM, sulfated glycosaminoglycans (GAGs), including heparan sulfate (HS) and chondroitin sulfate species, assure structural scaffold functions and relevant biological effects on cell growth, migration, and differentiation.[10] These regulatory roles are

[1]Faculté des Sciences et Technologie, Université Paris Est Créteil, Créteil, France.
[2]Laboratoire CRRET, EAC CNRS 7149, Université Paris Est Créteil, Créteil, France.
[3]Laboratoire Pathologies et Biothérapies de l'Organe Dentaire, EA2496, Université Paris Descartes, Montrouge, France.
[4]OTR3 SAS, Paris, France.
[5]Centre de Thérapie des Brûlures Graves, Hôpital d'instruction des armées Percy, Clamart, France.

related to their ability to interact with heparin-binding proteins (HBP) and to protect them from proteolytic degradation, increasing their half-life.[10] During osteogenesis, HS provide matrix-bound or cell surface-bound reservoirs for specific HBP, including growth factors, such as fibroblast growth factor-2 (FGF-2)[12] and bone morphogenic proteins (BMP),[13] chemokines, cytokines, and enzymes also (for review, see Cool and Nurcombe[11]). The structural complexity of HS, characterized by spatially discrete sulfated domains, confers to these GAG-specific physical and biochemical properties for each association with partners of the HBP family.[15] In injured tissues, enhanced glycanase activity is supposed to limit the capacity of these endogenous GAGs to protect HBP and so to alter their regulatory effects.[14]

As a new approach to associate the relevance of the chemical signatures of GAGs to their biological functions, a family of glycanase-resistant GAG mimetics, called heparan mimetics (HM), has been developed as structural and functional analogs of natural GAGs. Structural mimicry is related to the presence of sulfate and carboxylate moieties along their polysaccharidic chains.[16] These compounds have improved both the efficiency and quality of healing after local treatment in numerous animal models[17,18] and are currently used as medical devices for the treatment of skin and eye ulcers.[19] From a functional point of view, GAG mimetics are thought to replace natural GAGs destroyed by matrix endoglycosidases in injured tissues in where they stand as scaffolds that support the activity of HBP.[20] Thus, HM were able to accelerate the spontaneous bone-healing process observed in partial full-thickness calvarial defects[21] and to induce the repair of trephine skull defects in rats, in which no spontaneous healing occurs.[22] HM were also able to enhance endothelization of prothesis[23] neovascularization after skeletal muscular ischemia,[24] and reduction in myocardium infarct size.[25] These effects were partly explained by the interactions with HBP such as FGF-2[23] or vascular endothelial growth factor (VEGF).[26] Recently, we demonstrated that GAG mimetics modulate stem cell properties, since two different HM were able to mobilize hematopoietic stem cells *in vivo* and to enhance rat MSC clonogenicity, proliferation, migration, and osteogenic differentiation *in vitro*, according to their specific structural signatures.[27,28]

In this work, we developed a new tissue engineering product by combining bone substitutes and hMSC with the sulfated HM [OTR_{4120}], selected for its bone regenerative effects after local treatment[21,22] and its angiogenic properties.[26] First, we studied the potentiating effect of the HM [OTR_{4120}] on the ability of hMSC to proliferate, migrate, and differentiate into an osteogenic phenotype *in vitro*. Then, we developed TCP/HA ceramics engrafted with [OTR_{4120}] and evaluated the hMSC colonization efficiency on them *in vitro*. Finally, we evaluated the interest of [OTR4120] association to substitutes on bone formation induced by hMSC in an ectopic subcutaneous implantation site in immunodeficient mice. This ectopic model allows testing the osteoinductive, osteoconductive, and osteogenic abilities of a scaffold to induce bone formation, taken out of a bone matrix microenvironment and endogenous pro-osteogenic growth factors such as BMP that could mask the exact level of efficiency of the device.

Our data indicate that the GAG mimetic is stably associated to TCP/HA substitutes and to hMSC. This TCP/HA/hMSC/HM combination can effectively modulate the inflammatory response and vascularization *in vivo*. Interestingly, we showed that the mimetic was able to inhibit bone formation when implanted in an unnatural ectopic subcutaneous site, suggesting that GAGs can regulate the osteoblastic/osteoclastic balance when the bone substitutes are ectopically implanted.

Materials and Methods

GAG mimetic, heparin, HS, and growth factors

[OTR_{4120}] was obtained from OTR3, Inc. This derivative of dextran T40 (Sigma) contains the same degree of substitution in the carboxylate and sulfate residues than heparin.[16] The fluorescein-labeled derivative [OTR_{4120}]^{FITC} was prepared from dextran–FITC (Sigma) as previously described.[29] Heparin from porcine intestinal mucosa (Sigma) and HS from the bovine kidney (Sigma) were used as natural GAG controls and were cell culture grade. Recombinant human FGF-2 was prepared as previously described.[30]

hMSC culture

hMSC were separated from bone marrow nucleated cells obtained from patients undergoing routine total hip replacement surgery (Percy Military Hospital, Clamart, France) after informed consent. Primary cells were isolated from the supernatant of spongious bone fragments and expanded in a culture medium (CM) based on α-minimum essential medium (α-MEM) (Invitrogen) plus 10% fetal calf serum (FCS) as previously described.[31] The media were routinely changed twice a week. All experiments were performed with hMSC at passage 2. Each set of *in vitro* experiments (proliferation, migration, alizarin red staining, and flow cytometry analysis) was performed with the same expanded pool of hMSC from the same patient. A set of experiments have been performed three times independently from three hMSC primary cultures obtained from three independent human donors. *In vivo* studies have been performed separately with three distinct hMSC pools isolated from three new patients.

hMSC proliferation assay

hMSC were seeded at 1×10^3 cells/cm^2 in 24-wells plates. The day after, the CM was changed and supplemented or not with increasing concentrations (ng/mL) of [OTR_{4120}]; 100 ng/mL doses of T40, HS and Heparin were used as controls. Five days after, the cell growth rate was measured by the colorimetric MTT cell assay according to manufacturer's protocol (Sigma) using a standard curve of hMSC.

hMSC migration assay

Migration assays were performed in microchemotaxis Boyden's chambers (Corning Costar) as previously described.[32] Briefly, hMSC were harvested after 24 h of culture in a migration medium (MM) composed of the RPMI 1640 medium (Invitrogen) and 0.25% of bovine serum albumin (BSA Fraction V; Sigma). Then, 5×10^5 cells were loaded into the top chamber. The bottom chamber unit containing the MM was supplemented or not with an increasing concentration of [OTR_{4120}] and with 5 ng/mL FGF-2 or FCS as controls. The plates were incubated for 12 h at 37°C. Then,

the membranes were stained with May-Grünwald and Giemsa solutions, mounted, and photographed. The migrated cells were quantified on three separate areas per filter.

In vitro *osteogenic differentiation assay*

hMSC were seeded at 3×10^3 cells/cm^2 in six-well plates. The day after, the medium was replaced by the CM or an osteogenic induction medium (OS) composed of α-MEM plus 20% FCS (v/v), 0.1 μM dexamethasone, 10 mM β-glycerophosphate, and 0.05 mM ascorbic acid (all from Sigma). The media were supplemented or not with [OTR_{4120}] and changed twice a week. After 3 weeks, the cells were fixed in absolute ethanol and stained with 2% alizarin red solution. Alkaline phosphatase (ALP) membrane expression was analyzed by flow cytometry at day 14 using phycoerythrin (PE)-conjugated monoclonal anti-human ALP antibody (R&D Systems Europe). PE-conjugated isotypic antibody was used as negative control. Cell labeling was analyzed with an MACS Quant cytometer (Miltenyi Biotec).

Quantitative real-time polymerase chain reaction

Total mRNA was extracted with TRIzol® reagent (Invitrogen). DNase treatment was performed with a DNA-free kit (Applied Biosystems/Ambion, Austin, TX), and cDNAs were synthesized by Superscript® II Reverse Transcriptase (Invitrogen) according to the manufacturer's instructions. The primers were designed by Primer3 output software and obtained by Eurofins MWG (Germany). The following specific oligonucleotides were used as reaction primers: glyceraldehyde-3-phosphate dehydrogenase (*GAPDH*), NM_002046.3, forward 5′-TGC CTGATGAGACAGAGGTG-3′, reverse 5′-TCCACCTGGACAGGATTAGC-3′; *BMP-2*, NM_001200.2, forward 5′-TGTGTCCCGACAGAACTCAG-3′, reverse 5′-AC AACCCTCCACAACCATGT-3′; osteocalcin (*OC*), NM_199173.4, forward 5′-GTGCAGAGTCCAGCAAAGGT-3′, reverse 5′-TCCCAGCCATTGATACAGGT-3′; osteopontin (*OP*), NM_001040058.1, forward 5′-CGCAGACCTGACATC CAGTA-3′, reverse 5′-ATGGCCTTGTATGCACCATT-3′. cDNA real-time amplification was performed with FastStart Universal SYBR Green Master (Rox; Roche) by following the manufacturer's procedures and monitored with the ABI Prism 7900 Sequence Detection System (PerkinElmer/Applied Biosystem). All samples were amplified simultaneously in one assay run set with classical cycling and melting conditions. Amounts of cDNA were normalized to *GAPDH* ($\Delta CT = CT_{\text{gene of interest}} - CT_{GAPDH}$), since we previously validated that *GAPDH* gene expression was stable during hMSC culture under a basal medium (CM) and osteoblastic differentiation (OS) with or without [OTR_{4120}]. Moreover, we experimentally validated the 100% efficiency of all our primers in our conditions, with poor ($Ct > 38$) or no amplification in water control for each couple. Results are reported as relative gene expression ($2^{-\Delta CT}$).

Biomaterial functionalization and colonization

Cube-shaped (4×4×4 mm) bone substitutes (Ceraver) were made of TCP (65%) and HA (35%) with a mean pore size of 500 μm. To immobilize a GAG mimetic on TCP/HA,[33] the biomaterials were incubated 36 h at 50°C with [OTR_{4120}] solutions at 10 or 50 mg/mL in phosphate-buffered saline (PBS) 1× or with PBS 1× alone (GAG-free control). Functionalized scaffolds were washed twice with NaCl 1 M to eliminate the mimetics unbound to the bone substitutes. To colonize the biomaterials, 5×10^5 hMSC were incubated with the scaffolds in 100 μL for 3 h at 37°C. Cell-free scaffolds were incubated under similar conditions. Cell colonization was performed 1 day before *in vivo* implantation.

Biomaterial cell-loading measurement

Cell-loaded biomaterials were washed with PBS 1× and incubated with a lysis solution containing a Tris–EDTA buffer 1×, 0.1% Triton X-100, and 0.2 mg/mL proteinase K (Roche Applied Science) at 50°C 12 h. The samples were then treated with 3 freeze/thaw cycles under strong shaking and sonication. A fixed volume of each sample was incubated with the PicoGreen® dye from the Quant-iT™ PicoGreen dsDNA kit (Invitrogen). Optical densities (OD) associated to DNA amount were analyzed with a Fluoroscan II (Labsystems, Thermo Fisher Scientific) at 480 and 520 nm, for exciting and emission wavelengths, respectively. OD was then reported to the total number of hMSC, as compared to a standard curve of DNA amount prepared with an increasing number of hMSC according to the same Picogreen protocol.

GAG mimetic quantification

GAG mimetics were quantified in the coated biomaterials before their *in vivo* implantation (day 0) and at their recovery from animals 30 days after the implantation procedure. Surrounding connective tissues were eliminated by 0.2 mg/mL proteinase K (Sigma) and 0.1% Triton X-100 treatments, during 24 h at 56°C. Natural GAGs were eliminated with 4 mU chondroitinase ABC (Sigma) and nitrous acid successive treatments.[34] Selective quantification of GAG mimetic linked to bone substitutes were performed by the dimethyl methylene blue (DMMB) assay.[34]

In vivo *ectopic implantation*

Four experimental groups of bone substitutes, functionalized or not and colonized or not, were subcutaneously implanted into 7 weeks old female immunodeficient nude mice (Rj:NMRI-nu; Janvier): (1) TCP/HA alone; (2) TCP/HA/OTR_{4120}; (3) TCP/HA/hMSC and (4) TCP/HA/OTR_{4120}/hMSC. Three independent experiments were performed with four biomaterials per condition: two biomaterials per mice were implanted on two mice per group. Mice were anesthetized with 100 mg/kg ketamine (Virbac Santé Animale) and 10 mg/kg xylasine (Bayer). Biomaterials were implanted along the dorsal axis of the back skin in subcutaneous pockets created by 7 mm incisions. 8 weeks after implantation, mice were sacrificed, the back skin was incised and the connective tissues separated to expose the bone substitutes and the surrounding vascularization network. This protocol was approved by the Ethical Committee for animal experiments of the Army Biomedical Research Institute of Bretigny-sur-Orge. The nursery is entitled by the French Ministere de l'Agriculture and regularly controlled by the Nursery Facility Committee for conformity with European regulations on animal experiments. Panoramic digital views were obtained with a numerical color camera (PowerShot A650 IS; Canon). A binocular magnifier associated to a

camera (E8400; Nikon) was used to take four pictures for numerical segmentation analysis of the vessel tree. All biomaterials were recovered and fixed in 70% ethanol for histological analysis.

Histological analysis of bone substitutes sections

Biomaterials were dehydrated by gradient ethanol, cleared by xylene and embedded in methyl methacrylate resin (Merck). Sections with thickness of 5 μm were obtained using a Polycut E microtome (Leica) and then deplastified in 2-methoxyethyl acetate solution (Carlo Erba), dehydrated in graded ethanol solutions and cleared in water. Sections were stained with toluidine blue (pH 3.8) and visualized using standard light microscopy. ALP activity was detected using naphtol AS-TR phosphate and fast blue RR salt (Sigma) in Tris 0.1 M (pH 9), $MgCl_2$, dimethylformamide (Merck).[21] Enzymatic activity of tartrate-resistant acid phosphatase (TRAP) was detected using naphthol AS-TR phosphate, sodium tartrate, and fast red TR salt (all from Sigma) dissolved in acetate buffer 0.1 M (pH 5.2) with dimethylformamide.[35] Masson's trichrome staining was performed according to standard procedures.

Batch images statistical analysis procedure of vessel tree segmentation

Pictures of the capillar network were analyzed using an ImageJ software program developed to quantify elements associated to the vascularization tree. Images were pretreated to improve tree image detection. Briefly, background signal, lightning shadings and reflections were removed. Then, the channel exhibiting the maximum of absorbance at the vessels locations was segmented.[36] The resulting binary images, once reduced to the minimal structural level, were analyzed as a sum of segments, branches and nodes. A segmentwas classically delimited by two nodes. A branch was defined by one node and one extremity. Each detected segment and branch was characterized by its length and each image analysis was summarized as object counts and length parameters recorded into a batch table.[37]

Statistical analysis

Results were expressed as mean of values ± standard deviation (SD) of the mean from triplicate (*in vitro*) or quadruplicate (*in vivo*) values per condition per experiment, obtained from at least three independent *in vitro* and *in vivo* experiments. Statistical analyses were performed using the Student's *t*-test (unpaired two-tailed).

Results

[OTR_{4120}] potentiates proliferation and migration properties of hMSC in vitro

Addition of [OTR_{4120}] at increasing doses in the CM of hMSC induced significant increase in the cell proliferation rate (Fig. 1A), as illustrated during the first 5 days with a maximal 50% increase obtained with the 1000 ng/mL dose. [OTR_{4120}] was as efficient as HS or heparin (100 ng/mL) whereas dextran T40 showed no effect. Moreover [OTR_{4120}] induced a 3.5-fold increase in migrating cells per field with 100 ng/mL dose (Fig. 1B), as compared to control cells in FCS-free medium (CT). This increase was similar to that obtained with FGF-2 (threefold), whereas a maximal fivefold increase was obtained with 20% FCS positive control. These results indicate that [OTR_{4120}] is able to induce proliferation and migration properties of hMSC.

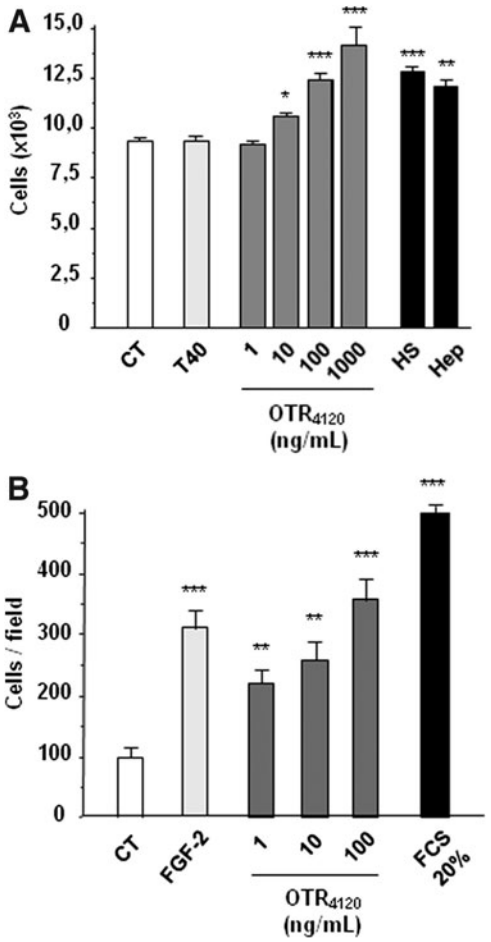

FIG. 1. The glycosaminoglycan (GAG) mimetic [OTR_{4120}] potentiates the human mesenchymal stem cell (hMSC) *in vitro* proliferation and migration properties. **(A)** hMSC proliferation was quantified using MTT assay after 5 days of treatment without (CT) or with increasing doses (ng/mL) of the GAG mimetic [OTR_{4120}] solubilized into culture medium and compared to 100 ng/mL of dextran (T40), natural heparan sulfates (HS) and Heparin (Hep). **(B)** The migration capacity of hMSC toward soluble [OTR_{4120}] was analyzed in the Boyden chambers assays for 12 h. Controls were performed in absence of fetal calf serum (FCS) as negative CT, and with 20% FCS and 5 ng/mL fibroblast growth factor-2 (FGF-2) as positive CT. Means ± standard deviation (SD) were obtained from triplicate per condition and per experiment, and from three independent experiments (*$p < 0.05$; **$p < 0.01$; ***$p < 0.001$).

[OTR_{4120}] induces osteogenic differentiation of hMSC in vitro

We tested the ability of [OTR_{4120}] to stimulate osteogenic phenotype on hMSC cultured in basal control (CM) or osteogenic (OS) medium for 21 days, as compared to the same conditions in absence of HM. Alizarin red staining of

calcium-rich deposits (Fig. 2A), indicative of functional osteocytes, was low in CM whereas additions of [OTR_{4120}] induced a clear increase in red staining intensity. In OS condition, the staining was strong and addition of [OTR_{4120}] had no effect. Similar effect was observed by flow cytometry analysis of cells expressing ALP marker at day 14 (Fig. 2B). In CM, 40% of cells were positive for ALP expression (ALP^+) and addition of [OTR_{4120}] (100 ng/mL) induced a twofold increase in ALP^+ cells. In OS condition 96% of cells were ALP^+ and addition of [OTR_{4120}] had no effect on this high level of expression. Next, the expression of osteogenic genes was analyzed by quantitative real-time polymerase chain reaction at day 7 and 14 of culture (Fig. 2C, D). Osteogenic gene expressions progressively increased between day 7 and 14 in OS medium. The treatment by [OTR_{4120}] significantly induced the expression of *BMP-2* in CM as well as in OS conditions. This inductive effect was also significant at day 7 for late markers, such as *OC* and *OP* that were not already induced in cells under the OS condition, suggesting that GAG mimetic treatment accelerate osteogenic gene expressions. Finally at day 14, [OTR_{4120}] treatment induce osteogenic gene expression to a lower extend than those obtained by OS medium, correlating results obtained with Alizarine Red staining and Flow cytometry analysis. Altogether, these results establish that [OTR_{4120}] is able to induce an osteogenic phenotype on hMSC in the absence of osteogenic medium.

[OTR_{4120}] coating on TCP/HA ceramics improve their colonization by hMSC in vitro

TCP/HA ceramics were functionalized with 10 mg/mL or 50 mg/mL [OTR_{4120}] solutions (A and B respectively), corresponding to 4 or 20 µg of mimetic incubated per cm^2 of ceramic surface respectively. DMMB assay performed at day 0 (Fig. 3A) indicated coated [OTR_{4120}] concentrations of 3.6 ± 0.4 ng/cm^2 (TCP/HA/OTR_{4120}-A) and 6.0 ± 0.7 ng/cm^2 (TCP/HA/OTR_{4120}-B) on the ceramic surface. These rate are

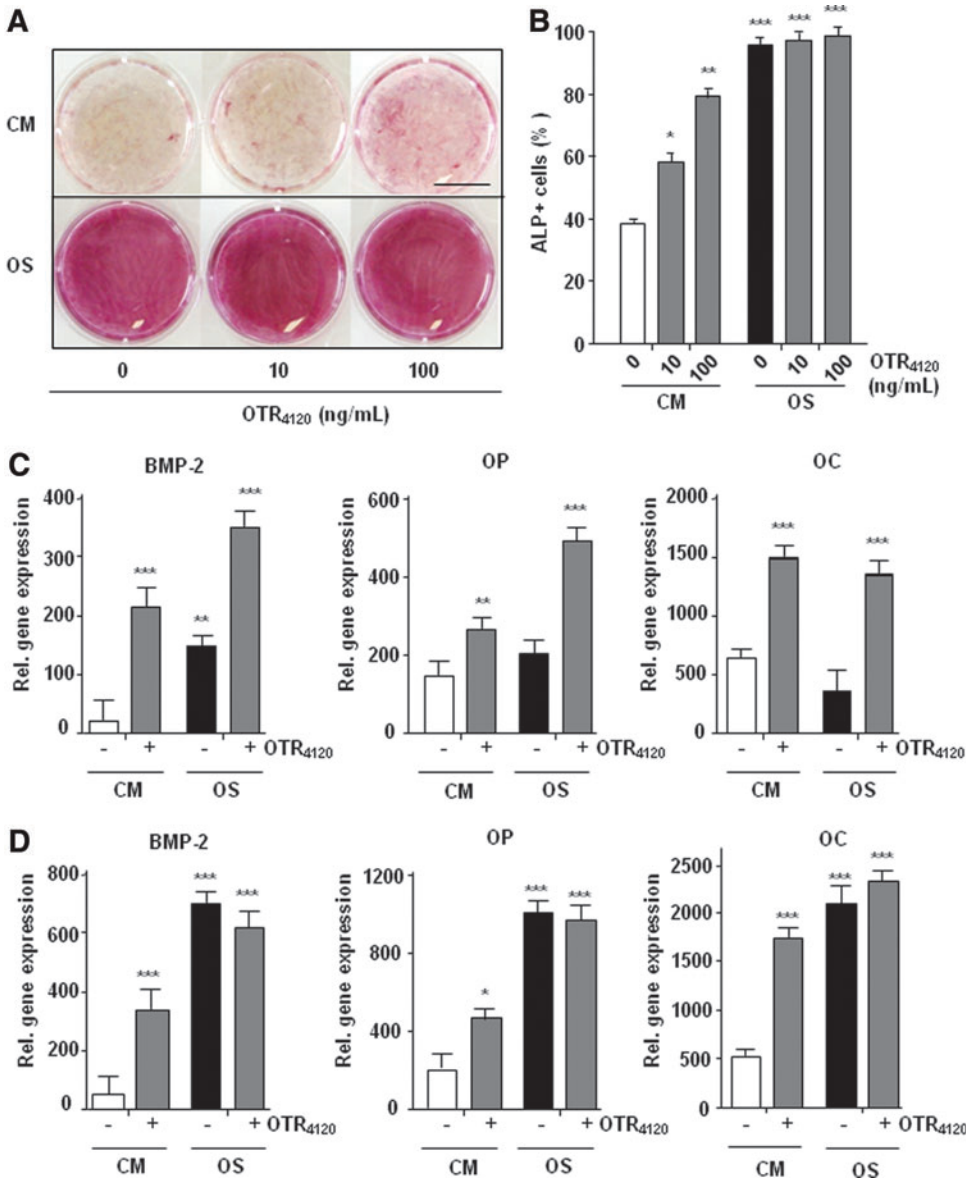

FIG. 2. The GAG mimetic [OTR_{4120}] potentiates the hMSC *in vitro* commitment to the osteogenic lineage. hMSC were expanded in a control (culture medium [CM]) or osteogenic (OS) medium supplemented or not with [OTR_{4120}] during 21 days. **(A)** Alizarin Red staining of the calcium deposits. Scale bar: 1 mm. **(B)** Flow cytometry analysis of alkaline phosphatase (ALP) expression. **(C, D)** Quantitative real-time polymerase chain reaction analysis of the expression of bone morphogenic protein-2 (*BMP-2*), osteocalcin (*OC*), and osteopontin (*OP*) after 7 days **(C)** and 14 days **(D)** of treatment. Expression levels are reported to glyceraldehyde-3-phosphate dehydrogenase (*GAPDH*) and presented as $2^{-\Delta Ct}$. Values are means ± SD of triplicate per condition and per experiment, from three independent experiments ($n = 9$; $^*p < 0.05$; $^{**}p < 0.01$). Color images available online at www.liebertpub.com/tea

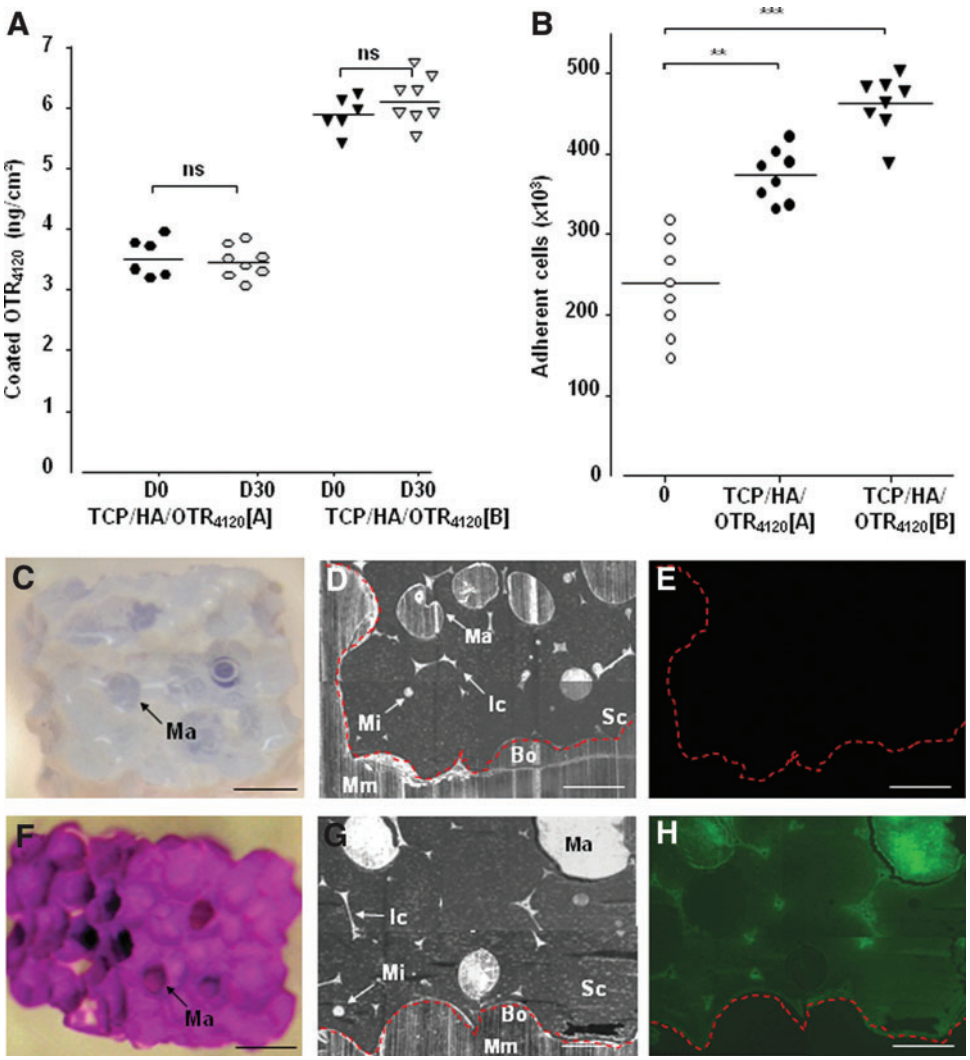

FIG. 3. The GAG mimetic [OTR_{4120}] functionalizes tricalcium phosphate/hydroxyapatite (TCP/HA) bone substitutes. Scaffolds were engrafted with 4 or 20 μg of [OTR_{4120}] per cm^2 of the TCP/HA-developed surface, TCP/HA/OTR_{4120} [A], and [B] scaffolds, respectively, or with phosphate-buffered saline 1× (negative control), and colonized by hMSC before *in vivo* implantation. Four weeks later, the scaffolds were harvested and treated enzymatically to eliminate proteins and endogenous glycans (GAG mimetics are resistant to these treatments). **(A)** The output of [OTR_{4120}] amount (ng/cm^2) covalently engrafted and quantified by the dimethyl methylene blue (DMMB) assay at day 0 before implantation (D0 black plots) and 30 days after *in vivo* implantation (D30 white plots) ($n=6$; $^{***}p<0.001$). **(B)** Colonization efficiency of scaffolds by hMSC (means of cell number ± SD) remaining into the scaffolds after 3 h of *in vitro* incubation before *in vivo* implantation (D0) and quantified with the fluorescent DNA probe Picogreen according to a standard curve of cells ($n=8$; $^{**}p<0.01$; $^{***}p<0.001$). **(C–H)** *In vivo* localization and stability of $[OTR_{4120}]^{FITC}$ engrafted on bone substitutes **(F, G, H)** compared to the control scaffolds without a GAG mimetic **(C, D, E)**. Scaffolds were treated for DMMB assay **(C, F)** and embedded in methyl methacrylate for analysis by phase-contrast microscopy **(D, G)** and fluorescence microscopy **(E, H)**. Red dotted line indicates outline of the scaffold. Ma, macropores; Mi, micropore; Ic, interconnection; Sc, scaffold; Mm, methyl methacrylate; Bo, border. Black scale bar: 1000 μm, white scale bar: 500 μm. Color images available online at www.liebertpub.com/tea

explained as the linkage reaction occur between the phosphate groups on the ceramic and the polysaccharides bearing a reactive reducing end, only available in 0.1% of the total amount of molecules.[16,33] Then these TCP/HA/OTR_{4120} scaffolds were analyzed for their ability to modulate hMSC colonization *in vitro* (Fig. 3B). Whereas only 42% of total cells (5×10^5 hMSC) were found on control scaffolds, cell colonization efficiency reached 80% for TCP/HA/OTR_{4120}-A and 90% for TCP/HA/OTR_{4120}-B. These results highlight that [OTR_{4120}] efficiently improve colonization of hMSC in functionalized scaffolds.

[OTR_{4120}] engraftment on TCP/HA ceramics is stable in vivo

To make sure the stability of the [OTR_{4120}]-engineered scaffolds as a matrix for extended period of time *in vivo*, TCP/HA substitutes functionalized with the $[OTR_{4120}]^{FITC}$ were subcutaneously implanted on immuno-deficient mice and compared to GAG-free substitutes as controls. The immobilized $[OTR_{4120}]^{FITC}$ was quantified by the DMMB assay (Fig. 3A) after optimized enzymatic and chemical removal of endogenous GAGs 30 days after *in vivo* implantation (D30).

The $[OTR_{4120}]^{FITC}$ amounts were quantified at 3.2 ± 0.3 ng/cm^2 (TCP/HA/OTR_{4120}-A) and 5.4 ± 0.4 ng/cm^2 (TCP/HA/OTR_{4120}-B) at D30 (Fig. 3A, white plots), which are similar values to those obtained before implantation (D0) (Fig. 3A, black plots). Macroscopic observation post-DMMB assay confirmed that no more endogenous GAGs were detected on control scaffolds that were colorless (Fig. 3C), whereas the GAG mimetics were still present on the functionalized scaffolds at D30, as revealed by the strong purple staining of the DMMB dye (Fig. 3F). Moreover, fluorescent analysis of the scaffold sections showed a homogenous distribution of the coated $[OTR_{4120}]^{FITC}$ (Fig. 3H) colocalized with both macropores and micropores (Fig. 3G), whereas no fluorescence was observed on a GAG-free scaffold (Fig. 3E). These results clearly demonstrated the GAG mimetics immobilized on the scaffolds are stable for at least 1 month *in vivo* and are resistant to potential mammalian glycanase digestion.

Effect of [OTR_{4120}] and hMSC associated to scaffolds on osteoformation in vivo

Four groups of scaffolds were analyzed for ectopic bone formation 8 weeks after implantation into nude mice: (1) TCP/HA alone; (2) TCP/HA/OTR_{4120}; (3) TCP/HA/hMSC; and (4) TCP/HA/OTR_{4120}/hMSC. Masson's trichrome staining was used to reveal the matrix organization and collagenic deposition, with bone formation characterized by green round nodules growing from the margin and connected to the biomaterial (Fig. 4A). ALP activity staining (ALP^+) was used to reveal osteoblastic precursor cells in purple, characterized by a fibroblast-like shape and a dense accumulation, and classically found around forming bone nodules (Fig. 4B). In parallel, bone nodule formation and ALP^+ areas were semiquantitatively evaluated (Table 1). Collagen deposition was noted around the TCP/HA/OTR_{4120} scaffolds as compared to TCP/HA alone (Fig. 4A). Similar collagen deposits were observed over the bone formation areas in the TCP/HA/hMSC sites; they were further increased in the TCP/HA/OTR_{4120}/hMSC scaffolds (Fig. 4A). No bone nodule formation or ALP^+ cell accumulation was noticed in the TCP/HA and TCP/HA/OTR_{4120} scaffolds (Fig. 4A, B respectively, and 0/12 values on Table 1). In contrast, bone nodules were observed, essentially located at the periphery of the constructs or into the most peripheral pores and interstices, in most the TCP/HA/hMSC scaffolds

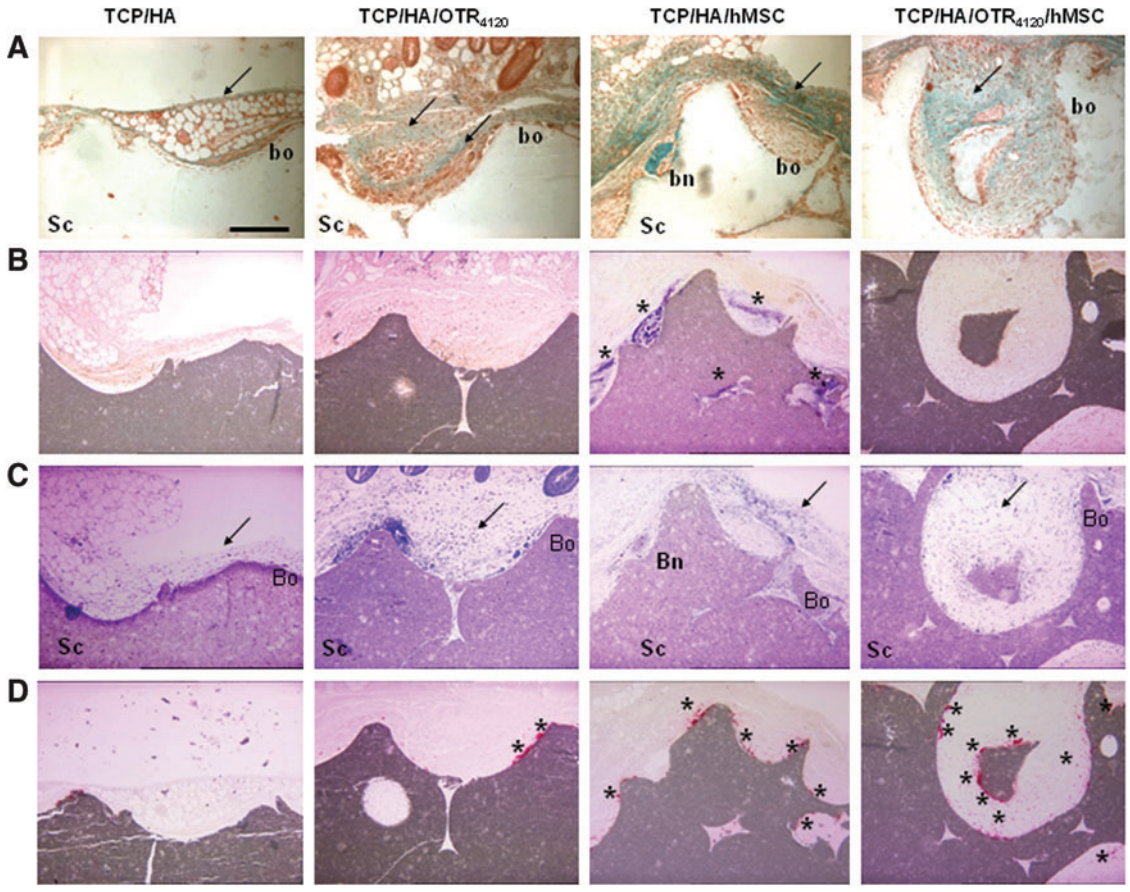

FIG. 4. The GAG mimetic [OTR_{4120}] immobilized on the TCP/HA substitutes inhibits bone formation induced by hMSC in the ectopic site. Controls and/or functionalized and/or cellularized scaffolds were implanted on mice and harvested after 8 weeks for histological study. **(A)** Masson's trichrome stain revealed the collagenic fibrillar tissue (*arrow*). **(B)** ALP activity staining showed violet areas with osteoblastic precursor cells (stars). **(C)** Toluidine blue staining indicated the host inflammatory response (*arrow*). **(D)** Tartrate-resistant acid phosphatase (TRAP) staining highlighted the red foci of osteoclastic cells (stars). Bn, bone nodule; Sc, scaffold; Bo: border. Scale bar: 200 μm. Pictures are representative of $n = 12$ samples (2 substitutes per mice × 2 mice × 3 independent experiments). Semiquantitative analysis of this histological study was reported in Table 1. Color images available online at www.liebertpub.com/tea

Table 1. Semiquantitative Analysis of Histological Studies

Device	*TCP/HA*	*TCP/HA/OTR$_{4120}$*	*TCP/HA/hMSC*	*TCP/HA/hMSC/OTR$_{4120}$*
Bone nodule + $n=12$	0/12	0/12	9/12	0/12
ALP areas + $n=12$	0/12	0/12	12/12	2/12
Inflammation index	1.91 ± 0.15^a	1.28 ± 0.18	2.46 ± 0.17^a	1.96 ± 0.26
TRAP + areas per device	20 ± 5	45 ± 7^a	46 ± 6^a	95 ± 3^b

The numbers of scaffolds exhibiting bone nodules and ALP-positive areas have been reported. The inflammatory tissue responses developed around each biomaterial have been semiquantitatively analyzed considering the cell layer thickness and the density of inflammatory cells on the periphery and inner pores. The intensity was reported on an inflammation index (scaled between 0 and 3). Osteoclastic activity was analyzed semiquantitatively by counting the number of TRAP+ cell foci per device. Values are means ± SD from $n=12$ samples (2 scaffolds × 2 mice × 3 independent experiments; $^a p<0.05$; $^b p<0.01$).

hMSC, human mesenchymal stem cells; TCP/HA, tricalcium phosphate/hydroxyapatite; ALP, alkaline phosphatase; TRAP, tartrate-resistant acid phosphatase; SD, standard deviation.

(9/12, Table 1) (Fig. 4A). All of them (12/12, Table 1) were clearly associated with ALP$^+$ cells (Fig. 4B). A decrease in the number of ALP$^+$ areas per sample (2/12, Table 1) along with a decrease in their size and staining intensity (Fig. 4B) occurred in the presence of [OTR$_{4120}$]. Further, no bone nodule was observed with this scaffold (Fig. 4A and 0/12 Table 1). Therefore, in the ectopic implantation site, the GAG mimetic, associated to ceramics, induced collagenic deposition without formation and calcification of the osteoid matrix even in the presence of hMSC.

Effect of [OTR$_{4120}$] and hMSC associated to scaffolds on the inflammatory response

Toluidine blue staining highlighted a layer of various cells types with cytological features of hematopoietic cells, including macrophages, giant cells, and neutrophils, around each type of implanted scaffold (Fig. 4C). These cells were observed in contact with all the TCP/HA surfaces, on which they initiated a resorption process, creating Howship-like cavities (Fig. 4C). However, the different constructs exhibited variations in the thickness and density of macrophages accumulation that we evaluated semiquantitatively according to a relative inflammation index (II) value at the periphery and in the macropores (Table 1). TCP/HA alone presented a dense layer of cells (Fig. 4C) quoted as 1.91 II value (Table 1). Association of hMSC to the scaffold (TCP/HA/hMSC) increased the II value to 2.46 (Table 1 and Fig. 4C); the macrophages were found between the substitute and the ALP$^+$ layer (Fig. 4B). However, when the scaffolds were functionalized with the mimetic, TCP/HA/OTR$_{4120}$ (Fig. 4C, 1.28 II value) and TCP/HA/hMSC/OTR$_{4120}$ (Fig. 4C, 1.96 II value), decreased inflammatory responses were observed in comparison with TCP/HA (Fig. 4C, 1.91 II value) and TCP/HA/hMSC (Fig. 4C, 2.46 II value), respectively.

Many cells in contact with the TCP/HA scaffold exhibited features of multinucleated giant cells Then, an histoenzymatic approach with TRAP staining was performed to characterize (Fig. 4D) and semiquantitatively evaluate (Table 1) a possible active participation of such clastic cell foci to resorption lacunas formation at the surface of the ceramic scaffold. A TRAP-positive (TRAP$^+$) staining was confirmed on the TCP/HA scaffolds with a homogeneous repartition around the biomaterial (Fig. 4D) and with a mean of 20 TRAP$^+$ foci per block (Table 1). The stained foci were twofold increased when the substitutes were associated with hMSC or [OTR$_{4120}$] (Fig. 4D and Table 1). A comparative survey of serial sections with ALP and TRAP staining indicated that clastic TRAP$^+$ areas (Fig. 4D) were found in the ALP-negative regions (Fig. 4C) and inversely. On TCP/HA/hMSC/OTR$_{4120}$ scaffolds, the TRAP$^+$ areas were clearly increased in intensity (Fig. 4D) and number, that is, fourfold compared to control (Table 1). These results suggest that the GAG mimetic association to scaffold stimulates the resorption foci.

Effect of [OTR4120] associated to scaffolds and hMSC on vascularization network

Once scaffolds had been removed from the animals, macroscopic differences were observed on the capillary bed surrounding the implantation site (Fig. 5A). The vascularization tree around TCP/HA was composed of few vessels, which failed to join the bone substitute. The addition of hMSC increased the skin vasculature network around the TCP/HA/hMSC implant. When [OTR$_{4120}$] was associated to the bone substitute, with or without hMSC, the vascularization network was denser. Moreover, in the presence of a mimetic, the vessel tree ramifications were more markedly orientated toward the functionalized substitutes, as compared to the TCP/HA/hMSC substitutes. On the light of these observations, we developed software to automatically analyze the vascularization tree extent after numerical captures (Fig. 5B, C). Two categories of objects, segments and branches, were defined to proceed to the analysis of the number and length of each ramification degree. Angiogenesis associated with hMSC engraftment was characterized by an increase in the number of segments and branches (Fig. 5D). However, functionalization of the scaffold with [OTR$_{4120}$], alone or in association with hMSC, significantly increased the number of terminal branches and segments, indicating that the GAG mimetic increased the ramification level. Same results were obtained on the lengths of each element (data not shown). These results validate the angiogenic potential of the GAG mimetic that allows important vascularization around the functionalized scaffold.

Discussion

In this study, we demonstrate that the GAG mimetic [OTR$_{4120}$] modulates the proliferation, migration, and osteogenic differentiation of hMSC *in vitro,* in agreement with

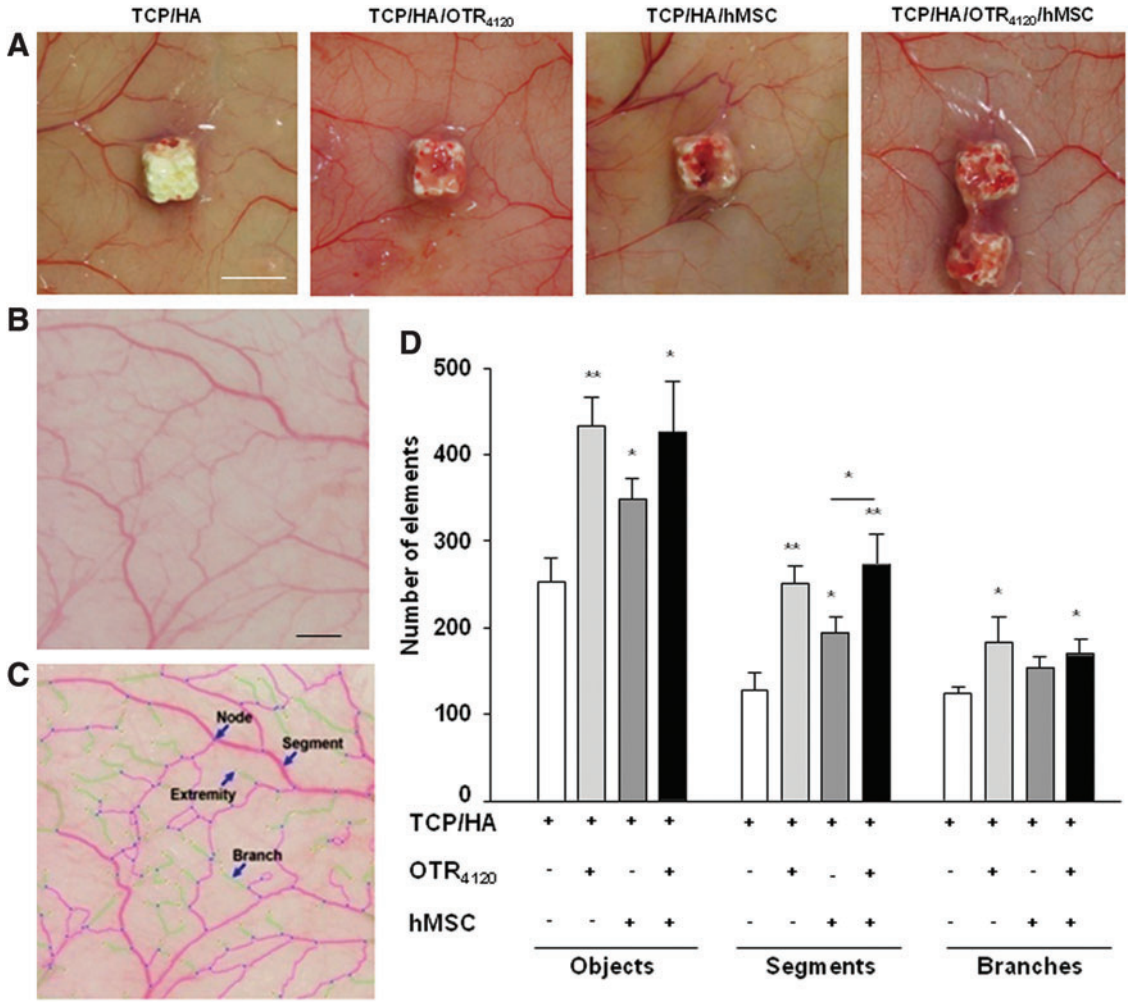

FIG. 5. The GAG mimetic [OTR_{4120}] immobilized on the TCP/HA substitutes potentiates the *in vivo* vascularization of the devices. **(A)** Macroscopic views of the capillary network surrounding each series of constructs. White bar: 5 mm. **(B, C)** Automatic computerized vessel tree segmentation decomposed the capillary areas in a sum of objects discriminating intermediary (segments) and terminal (branches) degrees of ramification before **(B)** and after **(C)** modelization. Black scale bar: 2 mm. **(D)** Automatic computerized quantification of the vascular element number. Data are mean values ± SD from $n = 12$ samples (4 cardinal areas per scaffold × 2 scaffolds per mice × 2 mice per conditions × 2 independent experiments; $^{*}p < 0.05$; $^{**}p < 0.01$). Color images available online at www.liebertpub.com/tea

our previous results on rat MSC.[28] Such modulating effects on hMSC properties could be due to a cooperative or protective effect of GAG mimetics on HBP present in the serum or secreted by MSC, such as FGF-2 and BMP. Accordingly, GAG mimetic derivatives were previously shown to modulate FGF-2, BMP-2, and TGF-ß activities on the MC3T3-E1 osteoblastic cell line derived from murine calvaria, possibly by regulation of these growth factor interactions with their membrane receptors.[39] Identification of associated factors is in progress to highlight the potential pathways involved in the GAG mimetic-promoting effects on primitive bone-forming cells such as MSC.

Since [OTR_{4120}] was able to stimulate human mesenchymal and endothelial cell[26] properties *in vitro*, we hypothesized that its association with bone substitutes could be of interest to mimic the matrix environment necessary for effective cell growth and differentiation during the bone formation process. Thus, we developed a methodology to engraft the polysaccharide to biphasic TCP/HA porous ceramics. Functionalized TCP/HA/OTR_{4120} was prepared with the mimetic distributed inside the pores and the interconnections of the synthetic substitutes as well as on the outside surface. The biological interest of this strategy was demonstrated by the significant increase in scaffold colonization by hMSC before implantation in mice. The analysis of $[OTR_{4120}]^{FITC}$-functionalized scaffolds harvested from animals demonstrated the mimetic stability for at least 1 month *in vivo*, and its resistance to host's proteases, glycanases, and inflammation mediators. Thus, we hypothesized that engrafting the linear sulfated GAG to bone substitutes would constitute an anchorage point for cells and a storage site for HBP. Then, as we demonstrated a chemoattractant effect of the soluble GAG mimetic on hMSC, we suggested that such properties could be retained by the engrafted GAG mimetic, resulting in improved migration of hMSC and increased cell colonization efficiency. Our results demonstrate that GAG

mimetics can be stably bound to the TCP/HA bone substitutes, resulting in functionalized medical devices with enhanced interactions with cells.

Ectopic osteoformation was further analyzed in immunodeficient mice after subcutaneous transplantation of TCP/HA bone substitutes, functionalized or not with the mimetic [OTR_{4120},] and associated or not with hMSC. Inflammatory response with formation of macrophage giant cells in the implantation site has already been reported in similar models, and could play a role on the transition to a chronic inflammatory reaction.[38] The cubic shape of the scaffolds could have perpetuated traumas and could explain such reaction. Interestingly, the TCP/HA/OTR_{4120} scaffolds were associated with a decrease in inflammation and an increase in collagen thickness, as previously described.[40,41] The anti-inflammatory effect of GAG mimetics has been related to their ability to increase collagen I and reduce collagen III accumulation and matrix metalloproteinase (MMP)-2 and MMP-9 proform inactivation, resulting in fibrosis reduction.[21,42] Previous works on crosslinking of natural GAG to collagen I matrices indicate that GAG protect porous lamellar matrix structures and modulate the host-tissue response through inhibition of giant cells and macrophage infiltrations.[43] Moreover, the presence of HS in these matrices also promoted angiogenesis. Thus, our data attest that GAG mimetics can readily be associated to bone substitutes to create an optimized matrix environment with enhanced biocompatibility and growth factor signaling capacity.

This ectopic subcutaneous bone formation model was validated with the TCP/HA substitute colonized with hMSC that can induce bone nodule formation and ALP^+ expression in a dense accumulation of osteoblastic cells. This observation also outlines the necessity to provide, *in situ*, osteoblastic progenitors to stimulate osteoformation. It was also shown that chemokine and growth factors secreted by MSC enhance wound healing through paracrine pathways inducing the recruitment of macrophages and endothelial cells.[44] In our TCP/HA samples, active ceramic resorption occurred in relatively small lacunae, excavating the smooth granule surface. This step, previously observed during the integration of various bone graft or bioceramics substitutes, is thought to gradually prepare the surface for collagen fibril and calcifiable matrix deposition[45] preliminary to subsequent bone formation. Mono- or plurinucleated cells responsible for such degradation had the morphological appearance of foreign-body giant cells and were positive for TRAP activity.[46] Interestingly, no bone nodule was observed in the TCP/HA (+/− hMSC) scaffolds functionalized with [OTR_{4120}], suggesting that this GAG mimetic inhibits any osteoblastic activity of engrafted hMSC in this ectopic model, whereas clastic activity was clearly increased. GAG, and particularly heparin, has been reported to influence osteoclastogenesis, but data remain very controversial, showing inhibitory[47–49] or stimulatory effects,[50,51] depending, for instance, on the doses, molecular weight, and sulfation patterns of the heparanoids. Preliminary *in vitro* experiments performed in our laboratory have indicated that [OTR_{4120}] is able to accelerate and potentiate differentiation of medullar monocyte/macrophage mononuclear cells toward multinucleated osteoclastic cells, under M-CSF and RANK-L treatment, comforting *in vivo* observation.

In contrast with these *in vivo* data suggesting resorption activity of a GAG mimetic in an ectopic site, previous studies reported a strong bone formation ability of GAG mimetics in orthotopic models. Indeed, in periodontitis and craniotomy-defect models, GAG mimetic treatments stimulated bone formation by promoting osteoprogenitor proliferation and differentiation and reduced bone resorption along with a decrease in $TRAP^+$ preosteoclast recruitment.[21,42] These osteoclastic effects (in ectopic model) versus osteoblastic effects (in orthotopic ones) could be linked to the physicochemical states of the GAG mimetic, depending whether they are free in solution or linked to protein core or scaffolds. We can hypothesize that GAG mimetics immobilized on scaffolds could have induced mobilization of hematopoietic progenitors, and monocytes, from the circulation, as previously shown after their intraperitoneal injection in mice.[27] GAG mimetics could act also as a reservoir of tissue-specific HBP, produced by either the therapeutic hMSC or the resident stem cells. In orthotopic models, GAG mimetics could be associated to tissue-specific distributions and concentrations of pro-osteogenic HBP and could stimulate bone formation, whereas pro-osteogenic HBP are lower, or even null in the ectopic model. Lastly, our results agree the reports in where GAG mimetics are described as tissue homeostasis regulators. In the orthotopic models, the GAG mimetics regenerated the injured tissues. In contrast, in the ectopic model, it is possible that the subcutaneous implantation induced a foreign-body reaction progressively eliminating the [OTR_{4120}]-coated scaffold, cellularized or not with hMSC, and reconstitute the original dermal tissue. This assumption would be in accordance with the conclusions of Luong-Van *et al.*,[38] which tested the association of natural HS with polyprolactone scaffold and predifferentiated hMSC in a similar ectopic model. If so, according to the homeostatic regulatory properties of a GAG mimetic, it would be preferable to implant the loaded substitutes within or close to bone tissue to enhance bone formation. The relevance of our *in vitro* data on the ability of [OTR_{4120}] to potentiate hMSC osteogenic properties and scaffold colonization suggests that GAG mimetics may provide a microenvironment suitable to enhance growth factor signaling, and ultimately bone formation if macroenvironment is permissive. It encourages testing further the TCP/HA/hMSC/OTR_{4120}-combined biomaterials in orthotopic bone regeneration models.

While the involvement of GAGs and particularly of HS activity on bone development was extensively validated, only few studies have already reported the successful use of natural HS molecules for bone therapeutic applications. The application of bone-derived HS into a mid-diaphyseal femoral fracture increased the trabecular bone volume by 20%.[52] However, in an ectopic model, the survival of the implanted cells was affected by the host response to the implant regardless of the presence of HS.[38] Whatever the discrepancies observed when using HS alone or associated to bone substitutes with therapeutic cells, it highlights the importance of the implantation site in the host response.

Another key point for future regenerative devices concerns the local angiogenic response after scaffold implantation. It is noteworthy that [OTR_{4120}] alone is able to modulate the vascular tree to the same extent as hMSC, but with a better organization. Modulation of angiogenesis by

GAG mimetics was previously observed in other lesion models[21] and was further validated by its ability to potentiate VEGF activity on endothelial cell properties. Here, we hypothesized that GAG mimetics are able to potentiate local VEGF or other angiogenic factors, secreted by resident or implanted cells.

Conclusion

Intelligent scaffolds are necessary to optimize bone formation. Most current strategies are based on specific growth factor induction of osteogenesis and angiogenesis. However, such therapeutic use of growth factors is limited by their susceptibility to degradation, the need to maintain prolonged local release at efficient levels, and the cost. Our results suggest that the GAG mimetic [OTR_{4120}] could be an alternative, since this stable compound, recognized to protect and potentiate HBP, is able to modulate hMSC properties *in vitro*. We showed here that engrafted to a biphasic ceramic scaffold, this mimetic improved the efficiency of hMSC scaffold colonization, which is a key parameter for successful biomaterial engraftment. Moreover, *in vivo* data showed an increased bone remodeling activity associated to GAG-engrafted scaffolds. This remodeling activity is associated to a modulated inflammatory response, which lead to inhibit bone formation on an ectopic dermal site. This work offers new perspectives for studying the effect of GAG mimetics on osteoclastic and angiogenic progenitors. In conclusion, our results indicate that GAG mimetics could find potential applications in bone therapy, since in addition to constitute matrix scaffolds to restore the injured ECM, they can effectively regulate key hMSC properties, angiogenesis process and bone remodeling, according to their ability to regulate tissue homeostasis. Further investigations in the orthotopic site will complete our knowledge on the GAG mimetic effect on bone formation and repair processes.

Acknowledgments

The G.F. doctoral fellowship was financed by Region Ile de France. This work has been supported by the Délégation Générale pour l'Armement (grant PEA No. 07coV02). We thank A. LLorens for helpful technical support. The authors are grateful to A. Destainville from Ceraver companies, which kindly provided TCP/HA ceramics.

Disclosure Statement

No competing financial interests exist.

References

1. Carson, J.S., and Bostrom, M.P. Synthetic bone scaffolds and fracture repair. Injury **38 Suppl 1,** S33, 2007.
2. Bielby, R., Jones, E., and McGonagle, D. The role of mesenchymal stem cells in maintenance and repair of bone. Injury **38 Suppl 1,** S26, 2007.
3. Chevallier, N., Anagnostou, F., Zilber, S., Bodivit, G., Maurin, S., Barrault, A., *et al.* Osteoblastic differentiation of human mesenchymal stem cells with platelet lysate. Biomaterials **31,** 270, 2010.
4. Ito, K., Yamada, Y., Nagasaka, T., Baba, S., and Ueda, M. Osteogenic potential of injectable tissue-engineered bone: a comparison among autogenous bone, bone substitute (Bio-oss), platelet-rich plasma, and tissue-engineered bone with respect to their mechanical properties and histological findings. J Biomed Mater Res A **73,** 63, 2005.
5. Niemeyer, P., Krause, U., Kasten, P., Kreuz, P.C., Henle, P., Sudkam, N.P., *et al.* Mesenchymal stem cell-based HLA-independent cell therapy for tissue engineering of bone and cartilage. Curr Stem Cell Res Ther **1,** 21, 2006.
6. Laschke, M.W., Harder, Y., Amon, M., Martin, I., Farhadi, J., Ring, A., *et al.* Angiogenesis in tissue engineering: breathing life into constructed tissue substitutes. Tissue Eng **12,** 2093, 2006.
7. Grellier, M., Bordenave, L., and Amedee, J. Cell-to-cell communication between osteogenic and endothelial lineages: implications for tissue engineering. Trends Biotechnol **27,** 562, 2009.
8. Roldan, J.C., Detsch, R., Schaefer, S., Chang, E., Kelantan, M., Waiss, W., *et al.* Bone formation and degradation of a highly porous biphasic calcium phosphate ceramic in presence of BMP-7, VEGF and mesenchymal stem cells in an ectopic mouse model. J Craniomaxillofac Surg **38,** 423, 2010.
9. Chen, F.M., Zhang, M., and Wu, Z.F. Toward delivery of multiple growth factors in tissue engineering. Biomaterials **31,** 6279, 2010.
10. Kim, S.H., Turnbull, J., and Guimond, S. Extracellular matrix and cell signalling: the dynamic cooperation of integrin, proteoglycan and growth factor receptor. J Endocrinol **209,** 139, 2011.
11. Cool, S.M., and Nurcombe, V. Heparan sulfate regulation of progenitor cell fate. J Cell Biochem **99,** 1040, 2006.
12. Dombrowski, C., Song, S.J., Chuan, P., Lim, X., Susanto, E., Sawyer, A.A., *et al.* Heparan sulfate mediates the proliferation and differentiation of rat mesenchymal stem cells. Stem Cells Dev **18,** 661, 2009.
13. Manton, K.J., Leong, D.F., Cool, S.M., and Nurcombe, V. Disruption of heparan and chondroitin sulfate signaling enhances mesenchymal stem cell-derived osteogenic differentiation via bone morphogenetic protein signaling pathways. Stem Cells **25,** 2845, 2007.
14. Handel, T.M., Johnson, Z., Crown, S.E., Lau, E.K., and Proudfoot, A.E. Regulation of protein function by glycosaminoglycans—as exemplified by chemokines. Annu Rev Biochem **74,** 385, 2005.
15. Turnbull, J.E., Miller, R.L., Ahmed, Y., Puvirajesinghe, T.M., and Guimond, S.E. Glycomics profiling of heparan sulfate structure and activity. Methods Enzymol **480,** 65, 2010.
16. Papy-Garcia, D., Barbier-Chassefiere, V., Rouet, V., Kerros, M., Klochendler, C., Tournaire, M., *et al.* Nondegradative sulfation of polysaccharides. Synthesis and structure characterization of biologically active heparan sulfate mimetics. Macromolecules **38,** 4647, 2005.
17. Colombier, M.L., Lafont, J., Blanquaert, F., Caruelle, J.P., Barritault, D., and Saffar, J.L. A single low dose of RGTA, a new healing agent, hastens wound maturation and enhances bone deposition in rat craniotomy defects. Cells Tissues Organs **164,** 131, 1999.
18. Barbier-Chassefiere, V., Garcia-Filipe, S., Yue, X.L., Kerros, M.E., Petit, E., Kern, P., *et al.* Matrix therapy in regenerative medicine, a new approach to chronic wound healing. J Biomed Mater Res A **90,** 641, 2009.

19. Chebbi, C.K., Kichenin, K., Amar, N., Nourry, H., Warnet, J.M., Barritault, D., *et al.* [Pilot study of a new matrix therapy agent (RGTA OTR4120) in treatment-resistant corneal ulcers and corneal dystrophy]. J Fr Ophtalmol **31,** 465, 2008.
20. Ikeda, Y., Charef, S., Ouidja, M.O., Barbier-Chassefiere, V., Sineriz, F., Duchesnay, A., *et al.* Synthesis and biological activities of a library of glycosaminoglycans mimetic oligosaccharides. Biomaterials **32,** 769, 2011.
21. Lafont, J., Blanquaert, F., Colombier, M.L., Barritault, D., Carueelle, J.P., and Saffar, J.L. Kinetic study of early regenerative effects of RGTA11, a heparan sulfate mimetic, in rat craniotomy defects. Calcif Tissue Int **75,** 517, 2004.
22. Lafont, J., Baroukh, B., Berdal, A., Colombier, M.L., Barritault, D., Caruelle, J.P., *et al.* RGTA11, a new healing agent, triggers developmental events during healing of craniotomy defects in adult rats. Growth Factors **16,** 23, 1998.
23. Desgranges, P., Barritault, D., Caruelle, J.P., and Tardieu, M. Transmural endothelialization of vascular prostheses is regulated *in vitro* by Fibroblast Growth Factor 2 and heparan-like molecule. Int J Artif Organs **20,** 589, 1997.
24. Desgranges, P., Barbaud, C., Caruelle, J.P., Barritault, D., and Gautron, J. A substituted dextran enhances muscle fiber survival and regeneration in ischemic and denervated rat EDL muscle. FASEB J **13,** 761, 1999.
25. Yamauchi, H., Desgranges, P., Lecerf, L., Papy-Garcia, D., Tournaire, M.C., Moczar, M., *et al.* New agents for the treatment of infarcted myocardium. FASEB J **14,** 2133, 2000.
26. Rouet, V., Hamma-Kourbali, Y., Petit, E., Panagopoulou, P., Katsoris, P., Barritault, D., *et al.* A synthetic glycosaminoglycan mimetic binds vascular endothelial growth factor and modulates angiogenesis. J Biol Chem 23, **280,** 32792, 2005.
27. Albanese, P., Caruelle, D., Frescaline, G., Delbe, J., Petit-Cocault, L., Huet, E., *et al.* Glycosaminoglycan mimetics-induced mobilization of hematopoietic progenitors and stem cells into mouse peripheral blood: structure/function insights. Exp Hematol **37,** 1072, 2009.
28. Nicoletti, A., Bartoloni, A., Sofia, V., Mantella, A., Nsengiyumva, G., Frescaline, G., *et al.* Epilepsy and toxocariasis: a case-control study in Burundi. Epilepsia **48,** 894, 2007.
29. Martelly, I., Singabraya, D., Vandebrouck, A., Papy-Garcia, D., Cognard, C., Raymond, G., *et al.* Glycosaminoglycan mimetics trigger IP3-dependent intracellular calcium release in myoblasts. Matrix Biol **29,** 317, 2010.
30. Courty, J., Dauchel, M.C., Caruelle, D., Perderiset, M., and Barritault, D. Mitogenic properties of a new endothelial cell growth factor related to pleiotrophin. Biochem Biophys Res Commun 15, **180,** 145, 1991.
31. Doucet, C., Ernou, I., Zhang, Y., Llense, J.R., Begot, L., Holy, X., *et al.* Platelet lysates promote mesenchymal stem cell expansion: a safety substitute for animal serum in cell-based therapy applications. J Cell Physiol **205,** 228, 2005.
32. Ponte, A.L., Marais, E., Gallay, N., Langonne, A., Delorme, B., Herault, O., *et al.* The *in vitro* migration capacity of human bone marrow mesenchymal stem cells: comparison of chemokine and growth factor chemotactic activities. Stem Cells **25,** 1737, 2007.
33. Chen, P.R., Chen, M.H., Lin, F.H., and Su, W.Y. Release characteristics and bioactivity of gelatin-tricalcium phosphate membranes covalently immobilized with nerve growth factors. Biomaterials **26,** 6579, 2005.
34. Barbosa, I., Garcia, S., Barbier-Chassefiere, V., Caruelle, J.P., Martelly, I., and Papy-Garcia, D. Improved and simple micro assay for sulfated glycosaminoglycans quantification in biological extracts and its use in skin and muscle tissue studies. Glycobiology **13,** 647, 2003.
35. Baroukh, B., Cherruau, M., Dobigny, C., Guez, D., and Saffar, J.L. Osteoclasts differentiate from resident precursors in an *in vivo* model of synchronized resorption: a temporal and spatial study in rats. Bone **27,** 627, 2000.
36. Tsai W. Moment-preserving thresholding: a new approach. Comput Vis Graph Image Proc, **29,** 377, 1985.
37. Carpentier G. Custom tab stat from results. Available at http://rsb.info.nih.gov/ij/macros/CustomTabStatFromResults.txt, 2007.
38. Luong-Van, E., Grondahl, L., Song, S., Nurcombe, V., and Cool, S. The *in vivo* assessment of a novel scaffold containing heparan sulfate for tissue engineering with human mesenchymal stem cells. J Mol Histol **38,** 459, 2007.
39. Blanquaert, F., Barritault, D., and Caruelle, J.P. Effects of heparan-like polymers associated with growth factors on osteoblast proliferation and phenotype expression. J Biomed Mater Res **44,** 63, 1999.
40. Mestries, P., Alexakis, C., Papy-Garcia, D., Duchesnay, A., Barritault, D., Caruelle, J.P., *et al.* Specific RGTA increases collagen V expression by cultured aortic smooth muscle cells via activation and protection of transforming growth factor-beta1. Matrix Biol **20,** 171, 2001.
41. Alexakis, C., Mestries, P., Garcia, S., Petit, E., Barbier, V., Papy-Garcia, D., *et al.* Structurally different RGTAs modulate collagen-type expression by cultured aortic smooth muscle cells via different pathways involving fibroblast growth factor-2 or transforming growth factor-beta1. FASEB J **18,** 1147, 2004.
42. Escartin, Q., Lallam-Laroye, C., Baroukh, B., Morvan, F.O., Caruelle, J.P., Godeau, G., *et al.* A new approach to treat tissue destruction in periodontitis with chemically modified dextran polymers. FASEB J **17,** 644, 2003.
43. Pieper, J.S., van Wachem, P.B., van Luyn, M.J.A., Brouwer, L.A., Hafmans, T., Veerkamp, J.H., *et al.* Attachment of glycosaminoglycans to collagenous matrices modulates the tissue response in rats. Biomaterials **21,** 1689, 2000.
44. Chen, L., Tredget, E.E., Wu, P.Y., and Wu, Y. Paracrine factors of mesenchymal stem cells recruit macrophages and endothelial lineage cells and enhance wound healing. PLoS One **3,** e1886, 2008.
45. Saffar, J.L., Colombier, M.L., and Detienville, R. Bone formation in tricalcium phosphate-filled periodontal intrabony lesions. Histological observations in humans. J Periodontol **61,** 209, 1990.
46. Hayman, A.R. Tartrate-resistant acid Phosphatase (TRAP) and the osteoclast/immune cell dichotomy. Autoimmunity **41,** 218, 2008.
47. Baud'huin M, Ruiz-Velasco, C., Jego, G., Charrier, C., Gasiunas, N., Gallagher, J., *et al.* Glycosaminoglycans inhibit the adherence and the spreading of osteoclasts and their precursors: role in osteoclastogenesis and bone resorption. Eur J Cell Biol **90,** 49, 2011.
48. Ariyoshi, W., Takahashi, T., Kanno, T., Ichimiya, H., Shinmyouzu, K., Takano, H., *et al.* Heparin inhibits osteoclastic differentiation and function. J Cell Biochem 15, **103,** 1707, 2008.
49. Ling, L., Murali, S., Stein, G.S., van Wijnen, A.J., and Cool, S.M. Glycosaminoglycans modulate RANKL-induced osteoclastogenesis. J Cell Biochem 15, **109,** 1222.

50. Irie, A., Takami, M., Kubo, H., Sekino-Suzuki, N., Kasahara, K., and Sanai, Y. Heparin enhances osteoclastic bone resorption by inhibiting osteoprotegerin activity. Bone **41,** 165, 2007.
51. Folwarczna, J., Sliwinski, L., Janiec, W., and Pikul, M. Effects of standard heparin and low-molecular-weight heparins on the formation of murine osteoclasts *in vitro*. Pharmacol Rep **57,** 635, 2005.
52. Jackson, R.A., McDonald, M.M., Nurcombe, V., Little, D.G., and Cool, S.M. The use of heparan sulfate to augment fracture repair in a rat fracture model. J Orthop Res **24,** 636, 2006.

Address correspondence to:
Patricia Albanese, PhD
Laboratoire CRRET
EAC CNRS 7149
Université Paris Est Créteil
94010 Créteil
France

E-mail: albanese@u-pec.fr

Received: June 15, 2012
Accepted: February 18, 2013
Online Publication Date: May 16, 2013